On the Remote Detection of Swell by Satellite Radar Altimeter

C. L. PARSONS

NASA Wallops Flight Center, Wallops Island, VA 23337

(Manuscript received 6 October 1978, in final form 21 May 1979)

ABSTRACT

A technique is presented whereby the presence of swell can be determined from satellites in orbit. Utilizing an empirical model developed during JONSWAP, a parameter is derived that is shown to be related to the percentage swell present as reported by National Weather Service hindcasters. Only data presently available from existing satellite radar altimeters are needed to map those areas of the oceans dominated by swell.

1. Introduction

Deep ocean waves that most prominently affect industries dependent on the ocean are in the gravity-wave frequency range. Within this band, it is frequently assumed that two types of surface wave can be distinguished. The wind-driven sea state is of higher frequency, with the waves steeper, rougher, and more confused than those designated as swell. Swell occurs when wind-driven waves escape from the influence of the generating wind.

Because of the frequency difference between these two kinds of gravity waves, they can be distinguished by measuring and analyzing the frequency spectrum of a deep ocean wave field. This requires highly sophisticated data handling and recording instrumentation and a stable platform, such as a monster buoy whose motion is isolated as much as possible from the measurement process. Spectral measurement systems have been installed on airplanes and measurements of wave frequency have been made. However, these remote techniques depend on instrumentation with enough resolution to distinguish individual wave profiles on the ocean's surface. The extension of most remote frequency spectrum measurement techniques to satellite altitudes is not possible because of this requirement for high spatial resolution. One satellite instrument with high resolution, the synthetic aperture radar (SAR), may eventually produce two-dimensional wave spectra but this is not yet a proven capability. The determination of the frequency of the dominant ocean surface waves by SAR will likely be demonstrated first. Knowledge of this parameter or its reciprocal, the dominant wave period, is important for many applications.

An alternative approach is taken in this paper. For more than three years, the radar altimeter onboard the Geodynamics Experimental Ocean Satellite (GEOS-3) has been making significant wave height (SWH) (Parsons, 1979) and wind speed (U) (Brown, 1979) measurements over the earth's navigable oceans. An empirically obtained parameter derived only from these two inputs will be shown to be related to the presence of swell. This parameter should be useful in locating the swell-dominated regions of the oceans.

2. Characterizations of swell

a. Hasselmann/Walsh parameter

Hasselmann *et al.* (1976) found during JONSWAP that the nondimensional peak frequency and the nondimensional variance or energy of the sea surface displacement were functions only of nondimensional fetch during periods of wave generation by the wind. If

$$\tilde{\xi} = g^2\xi/U^4 = \text{nondimensional variance of surface displacement,} \quad (1a)$$

$$\tilde{f}_m = f_m U/g = \text{nondimensional peak frequency,} \quad (1b)$$

$$\tilde{x} = gx/U^2 = \text{nondimensional fetch,} \quad (1c)$$

it was found that

$$\tilde{\xi} = 1.6\cdot 10^{-7}\tilde{x}, \quad (2)$$

$$\tilde{f}_m = 3.5\tilde{x}^{-1/3}. \quad (3)$$

The displacement variance ξ, is the integral of the gravity wave frequency spectrum over all frequencies and is related to the SWH by

$$\text{SWH} = 4\xi^{1/2}. \quad (4)$$

Using (4), (1c) and (1a) in (2) yields

$$\mathrm{SWH} = 1.6 \cdot 10^{-3} U \left(\frac{x}{g}\right)^{1/2}. \quad (5)$$

Furthermore, from the relationship

$$\sigma^2 = (2\pi f)^2 = 2\pi g/\lambda, \quad (6)$$

the wavelength of the dominant surface displacement λ_m can be computed from (3), (1b) and (1c):

$$\lambda_m = 0.013 \left(\frac{x^2 U^2}{g}\right)^{1/3}. \quad (7)$$

Walsh (1977) proposes the combination of the parameters λ_m and SWH into a single variable $\Gamma = \lambda_m/\mathrm{SWH}$ that characterizes the stage of development or age of an ocean wave field. Waves under the influence of a generating wind tend to be steeper suggesting that Γ will be small. The theory of Stokes suggests that the lower limit of Γ is 7. (Frequently, the reciprocal of Γ, the wave steepness δ, is found in the literature.) As the wave field ages, the sea state calms, the spacing between waves becomes larger but more regular, and the sea evolves into swell. Values of Γ of up to 100 are not uncommon under these conditions. To determine Γ using GEOS-3 data, Eqs. (7) and (5) are combined to result in

$$\Gamma = 138.44 \left(\frac{\mathrm{SWH}}{U^2}\right)^{1/3}. \quad (8)$$

If the sea is fully aroused and the sea state can be characterized by the Pierson-Moskowitz spectrum, then (8) indicates that $\Gamma = 38.3$ for full development.

b. Wave-height development parameter

A second way of characterizing the development of the sea, or synonymously the importance of swell, is by dividing the SWH at a point by the fully aroused SWH that would exist there under the influence of the existing wind given sufficient fetch and duration. Using the Pierson-Moskowitz fully aroused sea spectrum, this is expressed as

$$\gamma = 47.17\ \mathrm{SWH}/U^2. \quad (9)$$

Comparing (9) and (8), it is obvious that these two characterizations are not unique and only one, Γ, will be utilized to parameterize a given sea state.

c. Wave age parameter

Sverdrup and Munk (1947) were the first to attempt to relate Γ to the "wave age" defined to be $\beta = c/U$, where c is the phase velocity of the waves. Swell propagates at a velocity that cannot typically be a result of the existing wind speed U at a specific location. Hence, the older the wave, the larger the value of β. A value of 1.0, of course, indicates fully aroused seas. In that case, Sverdrup and Munk estimate that $\Gamma = 26.3$, significantly smaller than the value obtained using (8) and the Pierson-Moskowitz fully developed sea frequency spectrum. This cannot be accounted for at this time.

Because of the independent formulation of β, it would be advantageous to relate it with Γ. With only SWH and U measurements from the satellite this, unfortunately, is impossible.

d. Percentage swell parameter

Based on work by Pierson *et al.* (1955) among others, hindcasting and forecasting techniques have been developed over the years by which wind waves are manually propagated out of the wind generating conditions and dispersed by angular spreading as swell. Using frequency and direction filters, the amount of swell and wind-driven sea present at a point on the ocean can be estimated by these methods. By characterizing the total sea state (SWH) as the square root of the sum of the squares of these two wave heights, a percentage swell parameter can be defined as

$$S = \mathrm{SWELL/SWH}. \quad (10)$$

Because of the utilization of this manual forecasting technique in the past and at the present (WMO, 1976) and its advantage of specifically identifying the swell component in quantitative terms, it will be used to produce the primary "ground truth" data set used in this study to compare with the values of Γ or γ generated using GEOS-3 satellite measurements of SWH and U.

TABLE 1. Examples of Γ and S parameter values for developing and dispersing wave fields.

	Developing wave field				Dispersing wave field			
Parameter	A	B	C	D	E	F	G	H
Sea (m)	10	4.44	8	2	10	8	6	0
Swell (m)	0	0	6	6	0	6	8	10
SWH (m)	10	4.44	10	6.32	10	10	10	10
U (m s^{-1})	30	20	30	30	31.7	19.4	16.8	0
Γ	30.89	30.89	30.89	26.47	38.3	41.26	45.44	∞
S	0	0	0.6	0.95	0	0.6	0.8	1.0

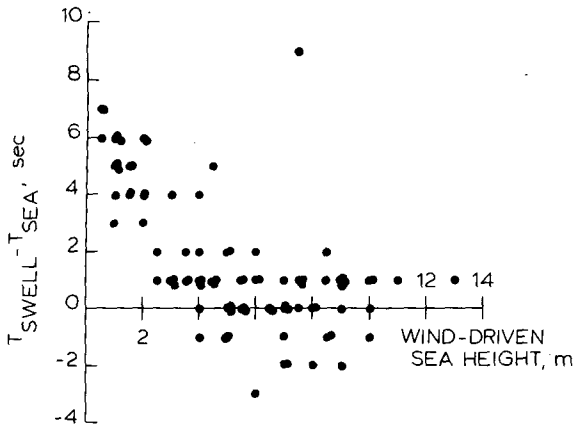

FIG. 1. The difference between reported periods of sea and swell from Ocean Weather Station *Lima* as a function of the wind-driven sea height.

3. Non-uniqueness of the Γ function

The Γ parameter can be applied to either developing or swell wave conditions but it is not a unique function of swell. This can be seen in Table 1 where several sets of sea state conditions are listed.

For a developing wave field, the non-uniqueness is quite evident. Cases A and B yield the same Γ and S values, but when swell is introduced in Case C, the value of S goes to 0.6 for the same Γ. In the extreme situation represented by Case D, the sea state is 95% swell but the Γ value is low at 26.47. This situation could result in a region of the ocean dominated by high swell which is suddenly whipped up by an approaching severe storm. In the interim between the time the high winds begin and the time when the sea becomes significantly developed, high values of S and low values of Γ are possible.

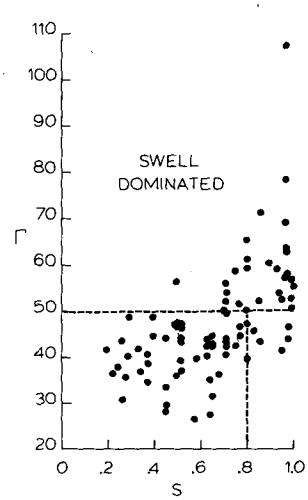

FIG. 2. The relationship of the Hasselmann/Walsh parameter Γ computed with GEOS-3 SWH and U measurements and the percentage swell parameter calculated using SPB sea and swell hindcasts. The location of the swell-no swell decision boundary Γ = 50 or S = 0.8 is also shown.

Case E represents the transition from a developing to dispersing wave field. Although $S = 0$ signifies the absence of swell, Γ = 38.3 shows that the sea is fully aroused. The removal of the wind would create a swell-dominated sea and the value of S would increase accordingly. The final three cases illustrate the common increase of both Γ and S. Because of the nonunique quality of Γ for developing wave conditions, the parameter can be considered only as a discriminator of swell dominated conditions. That is, Γ can realistically be used as a threshold detector of swell dominated conditions only and not as a continuous indication of sea state development. Using the definition of Γ, it can be shown that for values of Γ in excess of a selected decision threshold of 50 the amount of swell must exceed the fully arisen significant wave height that could exist given the ambient wind conditions. Hence, it can be stated unambiguously that if this decision threshold is exceeded then, barring undue interference from the noisiness of the data, the sea state at that point is dominated by swell.

4. Ground truth sources

To determine the usefulness of the Γ parameter introduced above, it is necessary to compare the Γ values produced by satellite altimeter measurements with ground truth measurements of sea state conditions. During February 1976, a concentrated scheduling effort resulted in the collection of a GEOS-3 data set that blanketed the North Atlantic Ocean for the entire month. This measurement base was collected and subsequently used to demonstrate the quality of the radar altimeter wave-height calculation process (Parsons, 1979) because of the wide range of SWH historically known to exist at that time and place. The ground truth data used in the previous study are also applicable here and each particular data set is described below.

a. Ship-board observations

Observations of sea wave height and period; swell wave height, period, and direction of propagation; and wind speed and direction were obtained from four fixed-position Ocean Weather Station (OWS) ships located and operating in the North Atlantic Ocean during the intensive data collection month. A close examination of these four data records has revealed inconsistencies that compromise the suitability of these observations for use as ground truth in this study. The observer at ship C, for example, located at 53.5°N, 35°W generally reported either sea or swell but not the two together. In contrast, the ship L observer always reported both. With inspection, however, it was found that

TABLE 2. Summary of data source error analyses.

Source	Sensor	Standard	Parameter	Error
Withee and Blasingame (1976)	NDBO Wave Spectra System	Lab tests, simulations and error analyses	U	± 0.3 m s^{-1}
			SWH	± 1.0 m
			Period	± 1.5 s
			Spectra	$\pm 50\%$
Parsons (1979)	GEOS-3	NDBO wave spectra system buoy	SWH	± 0.6 m
Brown (1979)	GEOS-3	NDBO wave spectra system buoy	U	± 2.1 m s^{-1}

the period reported for sea and swell were frequently the same. In Fig. 1, the difference between the two reports of wave period is plotted against the wind-driven wave height. For sea state of 5 m or more, this difference was near zero. Below 5 m SWH, the period was greater for swell than for the observed wind generated waves as expected. Although there undoubtedly is considerable value to be gained by utilizing the OWS data records for other purposes, on the basis of the previous discussion it was decided not to use the reports of swell as ground truth in this study.

b. NWS hindcasts

The other source of swell wave-height reports was the Special Projects Branch[1] (SPB) of the National Weather Service. Employing the techniques referred to in a previous section, the SPB provided estimates of wave height and period; swell height and period; and wind speed and direction at periodic intervals along each GEOS-3 groundtrack during February 1976. These data form the bulk of the ground truth data used in this study.

c. National data buoy report

Because no buoys were located in the North Atlantic during February 1976, measurements were not available to compare with the intensive GEOS-3 data set. However, reports of wind speed, wave height, and wave period have been obtained from the National Data Buoy Office (NDBO) for those buoys in the Gulf of Alaska which lay near GEOS-3 groundtracks during the past two years. The majority of the reporting buoys are now equipped with spectral measurement devices, but because of either the recent installation of such instruments or delays in the data processing and archiving of the spectral information, these reports have not been obtained at this time. When available, the buoy information will certainly be added to this study's ground truth data base.

The wave-period information that is available is not of sufficient quality for inclusion in these comparisons. For other applications, the wave spectra produced by the NDBO instrumentation are processed (Steele *et al.*, 1976) to yield measurements of wave period that have been shown (Cartwright and Longuet-Higgins, 1956) to relate to the number of zero crossings per unit time in the wave record. The higher frequency waves, of course, tend to bias the period computed in this fashion away from the period of the more energetic or dominant waves observed by the human eye that are more important for nautical operations. In the particular situation, where sea and swell both exist at some location, the NDBO computed period is generally near the value representative of the wind-driven portion of the frequency spectrum only. Hence, the presence of swell using these data can sometimes be completely overlooked.

5. Comparison of the Hasselmann/Walsh parameter with ground truth

In Fig. 2, values of Γ using GEOS-3 measurements of SWH and U in (8) are plotted against the

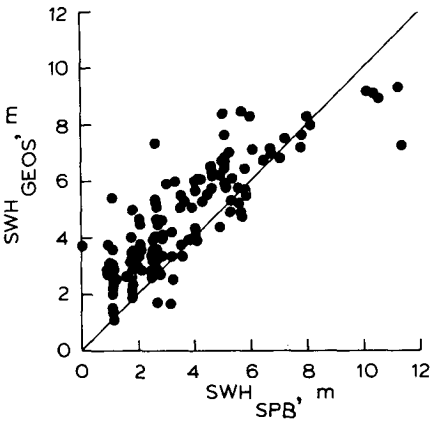

FIG. 3. The comparison of GEOS-3 SWH measurements with the corresponding SPB hindcasts of wave height.

[1] The Special Projects Branch was formerly named the Spaceflight Meteorology Group.

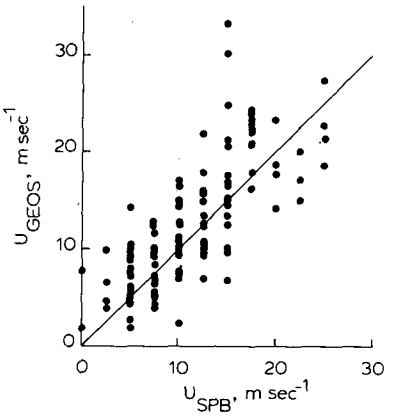

FIG. 4. The comparison of GEOS-3 wind speed measurements with SPB hindcasted values.

corresponding SPB hindcasts of sea and swell presented in the formula given by (10). Because of the way S is formulated, the scatter of points in Fig. 2 should identify a functional relationship that is asymptotic to the line $S = 1$ if Γ indeed is a function of S.

The scattering of data points is large but it can be seen that there is indeed a relationship whereby the larger Γ values do occur at higher values of S. Reasons for the noisiness of the data sets are discussed in a later section.

Because of the scatter and the non-uniqueness of Γ for developing seas as discussed previously, it is not prudent at this time to quantitatively express Γ in terms of S. Instead, a threshold value of Γ equal to 50 has been selected to serve as the decision boundary in a test for the presence or absence of swell. For $\Gamma = 50, S \approx 0.8$. That is, at the decision boundary, λ equals 50 times the SWH and swell accounts for 80% of the SWH. From the definition of SWH, this means that the wind-driven contribution is 60% of the SWH.

6. Discussion of scatter

The noisiness of the data in Fig. 2 is at first glance discouraging but after reconsideration understandable. The data from each source used in this study contains error. Other investigations have produced evaluations of these various errors to some degree. Pertinent studies are listed in Table 2. The Withee and Blasingame (1976) report, it should be noted, does discuss attempts to compare NDBO data with shipboard measurements. The error bounds on the windspeed measurements then increased to ± 1 m s^{-1}. The change is certainly due in part to shipboard inaccuracies but perhaps to open ocean environment effects on buoy performance as well. Both Parsons (1979) and Brown (1979) used buoy data to verify the performance capabilities of the GEOS-3 radar altimeter. In the case of the former intercomparison, the agreement between the satellite sensor and the buoy was within the performance specification expected of the buoy itself.

Figures 3 and 4 contain comparisons of GEOS-3 measurements of SWH and U, respectively, with the corresponding hindcast values from the SPB. Although the illustrations indicate that the satellite parameters are the dependent or unproven variables, the results shown in Table 2 tend to indicate the opposite. In terms of SWH, the SPB reports consistently underestimate the sea state. The wind speed comparison indicates little bias but large scatter about the 45° line of perfect agreement. Part of the smearing is due to the lack of resolution (2.5 m s^{-1}) in the hindcasts.

It is very difficult to quantify the errors in the hindcasting technique because of the qualitative way in which inputs to the hindcaster are utilized and the accuracy of these inputs. One type of error that significantly increases the scatter of both Figs. 3 and 4 has been discussed independently by Parsons (1979) and Brown (1979). As shown in Fig. 5, the

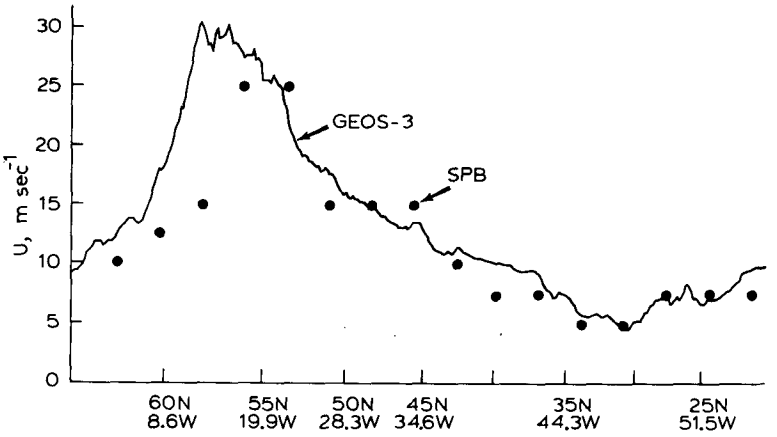

FIG. 5. The comparison of GEOS-3 wind speed measurements with the manually-produced SPB hindcasts for orbit 4532.

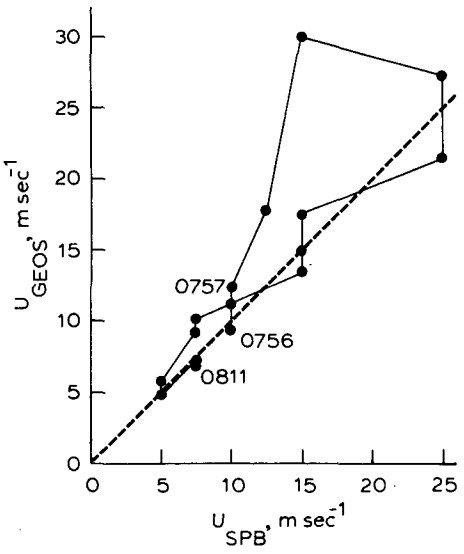

FIG. 6. The scatter plot representation of the satellite and hindcasted values of windspeed for orbit 4532 showing the "looping" effect of mislocation errors.

data records from the SPB frequently have features similar to the corresponding GEOS-3 records but misplaced in location along the satellite groundtrack. Notice that the region of high winds detected by the satellite between 58.2°N, 12.8°W and 53.8°N, 22.2°W also appears in the SPB data but is displaced nearly a minute of satellite travel time or 410 km southwest of the satellite determined position. As indicated in the references, this is likely to be the combined result of errors in the output of the National Meteorological Center (NMC) primitive equation model and a dearth of appropriately placed ship reports. The effect of this displacement on Figs. 3 and 4 is enormous. If the GEOS-3 wind speed (or wave height) measurements are plotted versus the corresponding SPB reports, then instead of a resulting straight line on or about the 45° line of perfect agreement, a loop will be created. Connected in time sequence, the data shown in Fig. 5 is plotted in this format in Fig. 6. Only the GEOS-3 reports collected at the time of the SPB hindcasts are shown, of course. If the displacement error were to place the high winds earlier in the hindcasts record than in the satellite data set, then the loop would be swept out in a counter-clockwise rotation. In the case of orbit 4532, the rotation is clockwise. It is obvious that many of the widely scattered points in Figs. 3 and 4 are the result of this error in placement of prominent weather features by the hindcaster.

The scatter in Fig. 2 is believed to be due to a combination of the accuracy limitations of the hindcast technique and the GEOS-3 radar altimeter and the errors that frequently occur in the inputs to the hindcaster such as the misplacement discussed above. Because the parameters Γ and S involve the ratio of these "noisy" measurements or estimates, the scatter of points in Fig. 2 is inevitable and unfortunately unavoidable at this time.

7. An example

Fig. 7 shows the 1200 GMT surface pressure analysis from the NMC for 24 February 1976 for the North Atlantic. The meteorology was dominated by a cold front that extended completely across the ocean with a low pressure system developing along the front at 51°N, 41°W. A strong pressure gradient existed to the south of the front from the longitude of the low to the British Isles. North of the

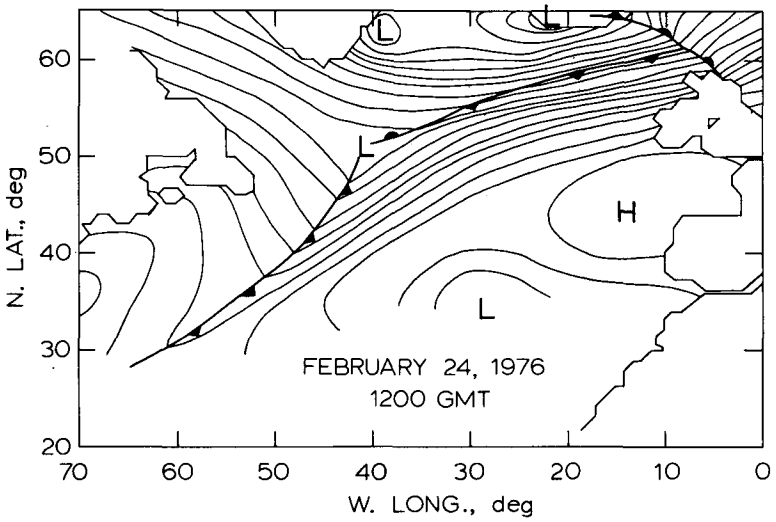

FIG. 7. The surface pressure analysis for the North Atlantic at 1200 GMT 24 February 1976.

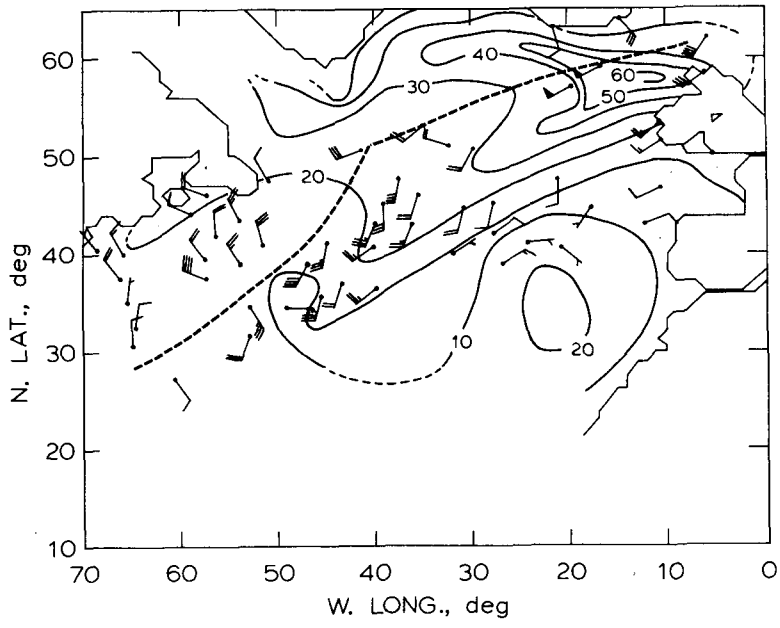

FIG. 8. The contour map of GEOS-3 measured surface wind speed for 1200 GMT 24 February 1976. The contour interval between the lines of constant wind speed (solid) is 10 kt. The dashed line indicates the location of the surface front and the ship reports plotted are those available to the hindcast analyst for this date and time.

front, another swath of strong pressure gradient stretched from southeast of Iceland to the tip of Greenland. Obviously, in the northeast sector of the North Atlantic considerable fetch existed on 24 February. Examination of the surface pressure analyses for the preceding days reveals that the storm system had slowly been progressing across the ocean in a southwest to northeast direction. Twenty-four hours before the map shown in Fig. 7, the low that is shown over Iceland was positioned at 54°N, 44°W. Hence, the region of the North Atlantic experiencing the strongest winds the preceding day was in that vicinity.

From GEOS-3, the inferred surface winds for 24 February 1976 have been compiled into one data set and contoured using the technique described by

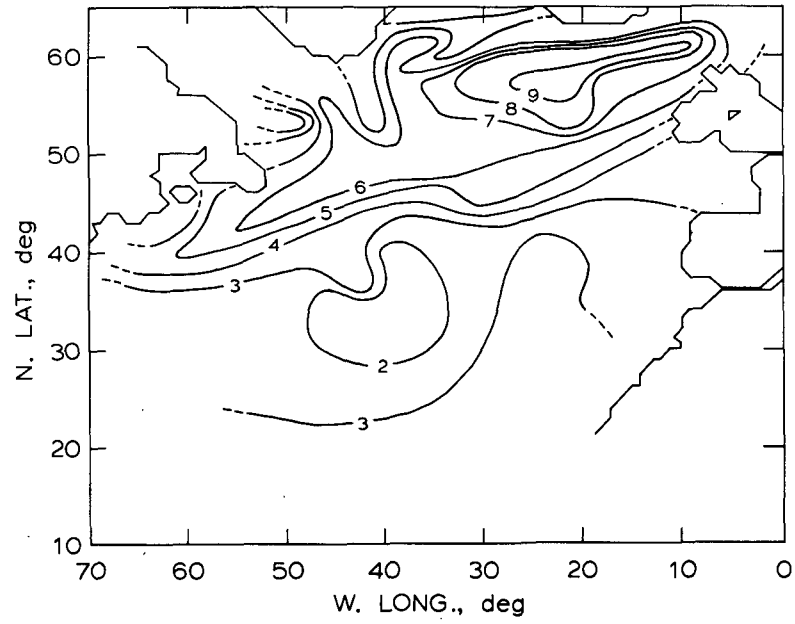

FIG. 9. The contour map of GEOS-3 measured significant wave height for 1200 GMT 24 February 1976. The contour interval is 1 m.

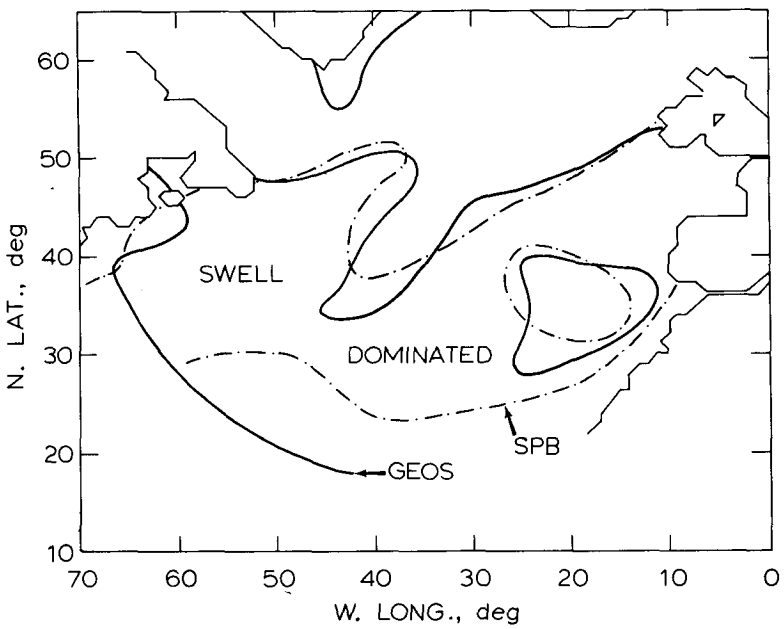

FIG. 10. The decision boundaries separating swell dominated regions from the remainder of the North Atlantic at 1200 GMT 24 February 1976. The solid line was constructed from the contour map of Γ computed using GEOS-3 measurements and the dashed line was extracted from the S map constructed from the SPB hindcasts.

Parsons (1979). The resulting map of U is shown in Fig. 8. The solid lines are isopleths of windspeed at a spacing of 10 kt, and the dashed line shows the position of the cold front as an orientation aid. There is an obvious tongue of high wind speed extending toward the southwest in the high-pressure gradient region south of the front and another band stretching east to west between Iceland and Greenland in complete agreement with the synoptic weather chart. The ship reports of wind speed used by the SPB hindcasters are shown in the figure also to illustrate the "fair weather" bias effect. Only three ship reports were available within the region bounded by the 30 kt contour line and only one inside the 40 kt line. This makes the determination of wind speed, wave height and storm location extremely difficult for the hindcast analyst.

A similar treatment is given in Fig. 9 for the composite GEOS-3 SWH data set for 24 February. In contrast to the position of the tongue of high wind speed in the preceding figure, the ridge of high SWH in this map lies further to the north. When the data shown in Figs. 8 and 9 are used in (8), a contour map of Γ can be made. Similarly, using SPB hindcasts of SWH and swell height in (10), a map of S can be constructed. In Fig. 10, only the boundaries $\Gamma = 50$ and $S = 0.8$ are shown. The agreement is quite good. It can be seen that the ridge of high SWH is wind-driven in its eastern portion but becomes swell-dominated at its western extent. This is exactly the region dominated by high winds 24 h prior to the time of this chart. The tongue of generating seas to the east of this feature is the region being influenced by the wind at 1200 GMT 24 February 1976.

For a cyclonic disturbance, the motion of the storm and the direction of its circulation tend to produce swell that propagates to the right of the storm's motion. This also is clearly seen in Fig. 10. Even the circular area of generating seas at 35°N, 20°W is reproduced by the SPB and GEOS-3 products.

8. Conclusions

A technique has been developed and discussed in this paper which utilizes only significant wave height and wind speed measurements available from the GEOS-3 radar altimeter in real time to locate swell dominated regions of the earth's oceans. Reasonable agreement exists between the GEOS-3 map of the North Atlantic for 24 February 1976 and a map produced from hindcasted values of sea and swell obtained from the Special Projects Branch of the National Weather Service. This example indicates that the decision boundary developed in this study to distinguish swell-dominated seas is a realistic choice.

REFERENCES

Brown, G. S., 1979: Estimation of surface wind speeds using GEOS-3 σ^0 (0°) measurements. *J. Geophys. Res.*, **84**, 3987–3989.

Cartwright, D. E., and M. S. Longuet-Higgins, 1956: The

statistical distribution of the maxima of random function. *Proc. Roy. Soc. London,* **A237,** 212–232.

Hasselmann, K., D. B. Ross, P. Muller and W. Sell, 1976: A parametric wave prediction model. *J. Phys. Oceanogr.,* **6,** 200–228.

Parsons, C. L., 1979: GEOS-3 wave height measurements: An assessment during high sea state conditions in the North Atlantic. *J. Geophys. Res.,* **84,** 4011–4020.

Pierson, W. J., Jr., G. Neumann and R. W. James, 1955: Practical methods for observing and forecasting ocean waves by means of wave spectra and statistics. U.S. Navy Hydrographic Office Pub. No. 603, 284 pp.

Steele, K. E., A. Trampus, P. A. Wolfgram and B. S. Graham, 1976: An operational high resolution wave data analyzer system for buoy. *Proc. Second Annual Combined Conf.,* Mar. Tech. Soc. and IEEE, 14B1–14B9.

Swerdrup, H. V., and W. H. Munk, 1947: Wind, sea, and swell: Theory of relations for forecasting. U.S. Hydrographic Office Publ. No. 601, 44 pp.

Walsh, E. J., 1977: Limitations on oceanographic use of beam-limited target-referenced radars. *IEEE Trans. Antennas Propagat.,* **AP-25,** 312–318.

Withee, G. W., and W. C. Blasingame, 1976: Environmental data quality estimates for ocean data buoys. *Proc. Second Annual Combined Conf.,* Mar. Tech. Soc. and IEEE, 14F1–14F6.

World Meteorological Organization, 1976: *Handbook on Wave Analysis and Forecasting.* WMO Publ. No. 446, 74 pp.